JOURNAL OF THERMOPHYSICS AND HEAT TRANSFER
Vol. 14, No. 1, January–March 2000

Aerodynamic Drag Reduction by Plasma and Hot-Gas Injection

Y. C. Ganiev,* V. P. Gordeev,* A. V. Krasilnikov,† V. I. Lagutin,* V. N. Otmennikov,* and A. V. Panasenko*
Central Research Institute of Machine Building, Russian Space Agency, 141070, Korolev, Moscow Region, Russia

The influence of plasma and hot-gas injection from a model's surface toward the external flow on aerodynamic drag of the model is researched. Experimental tests are conducted in transonic and supersonic wind tunnels at Mach numbers $M_\infty = 0.59$–4. Numerical experiments are carried out using unsteady Euler equations of an ideal perfect gas in integral conservative form. The calculations were performed at the oncoming Mach number $M_\infty = 4$, constant jet stagnation pressure, and jet stagnation temperatures of 600, 2000, and 6000 K. The investigations showed that the plasma or hot-gas injection can be used to reduce drag at subsonic, transonic, and supersonic Mach numbers, resulting in twice (or more) drag reduction. The calculations are in general agreement with the experimental data. The amount of drag reduction depends on jet stagnation temperature.

Nomenclature

C_d = drag coefficient
M_∞ = freestream Mach number
p = pressure, atm
q = freestream dynamic pressure, $\rho_\infty V_\infty^2 / 2$
S = area, m^2
T = temperature, K
t = time, s
V = velocity, m/s
ρ = density, kg/m^3

Subscripts

j = jet
0 = stagnation parameter
∞ = freestream

Introduction

AIRCRAFT drag reduction is a very real and important problem. Fuel is now half of the aircraft's base weight and even more than that for rockets. A 1% drag decrease leads, approximately, to a 10% increase in aircraft passengers payload or increased range. For many decades the aviation slogan has been "to fly higher and faster," and the point has been reached that drag reduction by means of finding optimal configurations has been practically exhausted. Therefore, we have begun to develop new technologies.

Supersonic aerodynamic drag can be reduced by mounting a needle or by injecting a gas jet at the tip of the aircraft nose.[1] Regulation of the needle position or the injected gas pressure permits both a considerable surface pressure redistribution and a reduction in the drag coefficient. The effect is attained as a result of the formation of flow separation zones ahead of the body, where the pressure is lower than behind the separated shocks ahead of analogous bodies without a needle or gas injection.

The model drag can be reduced as a result of the formation of a narrow rarefied channel ahead of the body.[2] The numerical calculation carried out for supersonic flow past a sphere in the presence of external heat release sources showed that the wave drag can be reduced by approximately 50–60% (Refs. 3 and 4). The effect of an electric discharge in front of an axisymmetric body on the supersonic flow was studied in Refs. 5 and 6. Many reports on that subject were made at 1st and 2nd Weakly Ionized Gases Workshops in 1997 (Colorado Springs, Colorado) and in 1998 (Norfolk, Virginia).[7,8]

Earlier, Finley described a series of experiments in which a single cold jet issued from an orifice at the nose of a body in supersonic flow to oppose the mainstream.[9] Using these data he developed an analytical model of flow that suggests that the aerodynamic features of a steady flow depend primarily on a jet flow-force coefficient and the Mach number of the jet in its exit plane.

In this paper we present the experimental and theoretical study of reducing aerodynamic drag by employing plasma and hot-gas injection conducted during the last several years beginning from our first publication[10] on this subject. The various results we have reported previously are in Refs. 11–13.

Experimental Facilities

The tests were conducted in supersonic and transonic wind tunnels. The specifications of the wind tunnels are given in Table 1.

Model with Built-In Plasma Generator

To conduct the studies we designed and manufactured a cone–cylinder model with a built-in plasma generator and strain gauges. In Fig. 1 the model is shown schematically. The barlike uncooled copper electrodes are embedded in a fluoroplastic insulator. The latter is inserted into a ferromagnetic-steel housing and fastened by three set screws. The clearance between the housing and insulator is sealed with a rubber ring. The plasma generator nozzle is connected with the housing by a ferromagnetic-steel adapter. The adapter-nozzle and adapter-housing connections are threaded and are sealed with rubber rings. The nozzle is made of copper. The inner surfaces of the housing and adapter are coated with electrical insulation.

A tap is introduced into the insulator to measure the pressure in the plasma generator chamber. An arc discharge is initiated by short circuiting the electrodes with a thin copper wire. The electrodes are connected to the three-phase 380-V ac mains via an automatic circuit breaker.

The plasma generator was mounted on a sting installed in the wind-tunnel working section, and the model-tubular strain gauge assembly was fitted on it. The strain gauges were fixed to the plasma generator housing with set screws. When voltage is fed to the electrodes, an electric arc is started. Driven by the electrodynamic forces, it moves toward the electrode ends, heats the gas in the plasma generator housing, is blown out of the interelectrode gaps, and breaks up. The plasma generator has the following major characteristics: the working section is up to 120 mm long, the interelectrode gaps are 10 mm wide, the electrode diameter is 4.5 mm, the short circuiting wire diameter is 0.4 mm, the inner diameter of the arc chamber is 30 mm, the nozzle throat diameters are 2 or 4 mm, the exit diameters are 5.65 and 7.61 mm, respectively, and the discharge current and time are approximately 300 A and 0.05, respectively.

Presented as Paper 99-0603 at the AIAA 37th Aerospace Sciences Meeting, Reno, NV, 11–14 January 1999; received 18 March 1999; revision received 18 June 1999; accepted for publication 18 June 1999. Copyright © 1999 by the American Institute of Aeronautics and Astronautics, Inc. All rights reserved.

*Ph.D. and Leading Research Associate, Aerodynamics Department.
†Professor and Head Scientist, Aerodynamics Department; kras@kiam.ru.

The model, in the form of a thin-walled cylinder–cone shell with a front vertex angle of 30 deg, is mounted on six-component aerodynamic strain gauges that are fastened to the tubular plasma generator housing. There are small clearances between the front of the model and the plasma generator nozzle housing, as well as between the rear portion of the model and the afterbody fairing. The effect of gas penetration into the model interior on the measured drag was considerably reduced by making the front clearance much smaller than the rear clearence.

In choosing the strain gauges, preference was given to tubular multicomponent dynamometers with short, and hence stiff, elastic elements whose aspect ratio was less than unity.

The pressure in the plasma generator chamber was measured using an inductive transducer. The oscillograms showed that an increase in the nozzle throat diameter results in the maximum pressure decreasing by a factor of 1.5 (Ref. 10). The plasma efflux time also decreases. For the nozzle throat diameter $d = 2$ mm, the maximum pressure in the plasma generator chamber was 15.4 atm, and for $d = 4$ mm, it was 9.7 atm.

Experimental Results for Model with Plasma Generator

Shadowgraph

A series of shadowgraph photographs was obtained to study flowfield structure change prior to and at the instant of plasma discharge. The photographs were taken using an IAB-451 shadowgraph (by the circular knife-edge method) and a movie digital color camera shooting at 2000 frames per second with an exposure of about 42 μs. Figures 2–6 show the results of these experiments for the conditions presented in Table 1. The first frames in Figs. 2–6 show the flow past the model prior to plasma discharge, and the second ones show the flow at the instant of plasma discharge from the internal plasma generator.

All tests were conducted with a plasma generator nozzle throat diameter of 4 mm except Mach 4, which was conducted with a nozzle throat diameter of 2 mm. At Mach 4 (Fig. 2), in the first frame, one sees an ordinary shock wave configuration, but at the instant of plasma discharge, one observes the decomposition of the original bow shock wave, the formation of the plasma ball in front of the model, and the formation of a new shock wave configuration.

At Mach 1.18 (Fig. 3), by comparing photographs prior to and at the instant of plasma discharge, one can see that the plasma jet moves the bow shock wave forward significantly.

At Mach 0.96 and 0.89 (Figs. 4 and 5), the bow shock wave is absent, and one can observe the changing of the λ-shock wave configuration only. The plasma jet influences the entire forehead model in these cases. The same also may be observed at the subsonic Mach number of 0.59 (Fig. 6).

Table 1 Wind tunnel specifications

Wind tunnel	Supersonic	Transonic
Test section dimensions, m	0.4 × 0.4	0.6 × 0.6
Mach number	4	0.59, 0.89, 0.96, 1.18
Reynolds number $\times 10^6$ for $L = 1$ m	2.8	0.82 ÷ 1.13

After looking through all of the photographs, it is possible to conclude that the flow near the model could be very changed by injecting plasma into oncoming subsonic, transonic, and supersonic flows.

Strain Gauges Measurements

Figures 7–11 present the experimental time dependence of the drag coefficient C_d for plasma flowing from a plasma generator nozzle at the same Mach numbers as for Figs. 2–6. The drag coefficients were calculated using the measured drag, the flow parameters, and the geometrical characteristics of the model. The data were recorded on a computer using a RWS 3072 amplifier with 0.1 accuracy rating. The signals were received and processed with the help of the FLEXLAB program module.

Figures 7–11 demonstrate the large drag reduction (from approximately two to four times) that correlates with the large flow changes of the photographs. The values of drag are practically the same prior

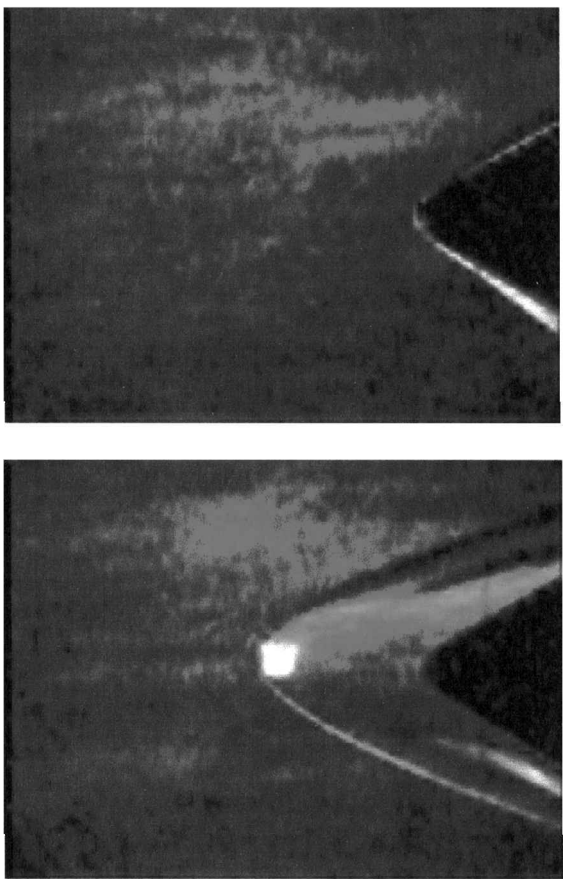

Fig. 2 Shadowgraphs at $M_\infty = 4$ prior to (top) and at the instant of plasma discharge.

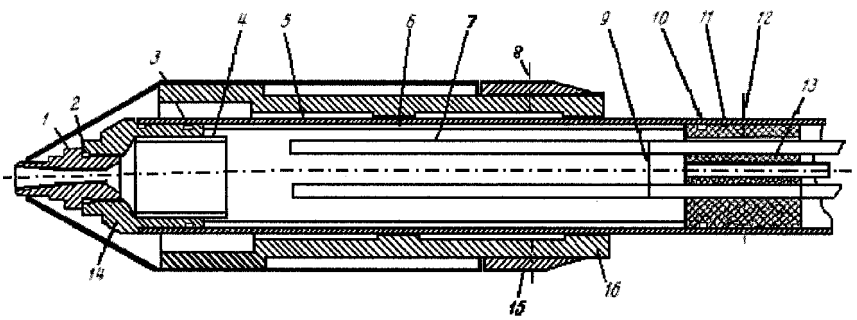

Fig. 1 Model with built-in plasma generator: 1, nozzle; 2, 3, and 10, rubber rings; 4 and 6, electrical insulators; 5, housing; 7, electrodes; 8 and 12, set screws; 9, thin copper wire; 11, fluoroplastic insulator; 13, pressure tap; 14, adapter; 15, afterbody fairing; and 16, strain gauges.

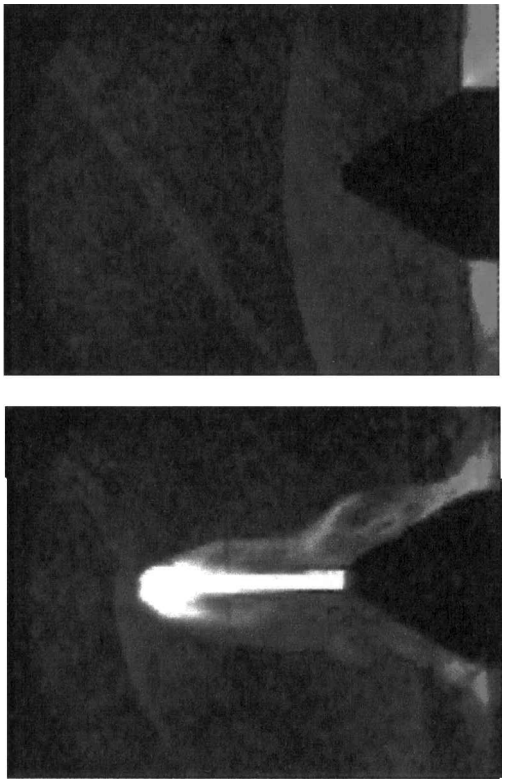

Fig. 3 Shadowgraphs at $M_\infty = 1.18$ prior to (top) and at the instant of plasma discharge.

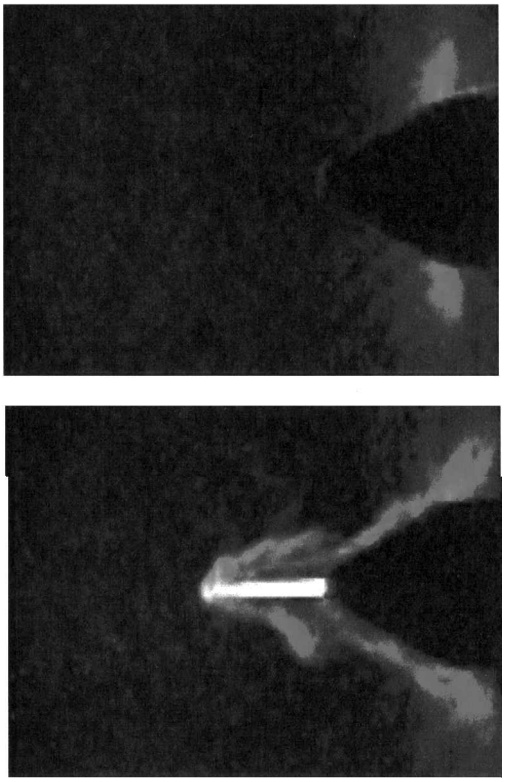

Fig. 5 Shadowgraphs at $M_\infty = 0.89$ prior to (top) and at the instant of plasma discharge.

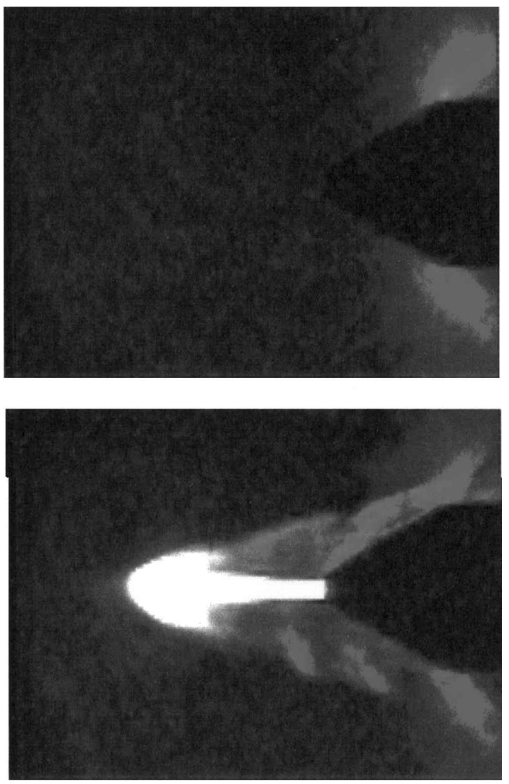

Fig. 4 Shadowgraphs at $M_\infty = 0.96$ prior to (top) and at the instant of plasma discharge.

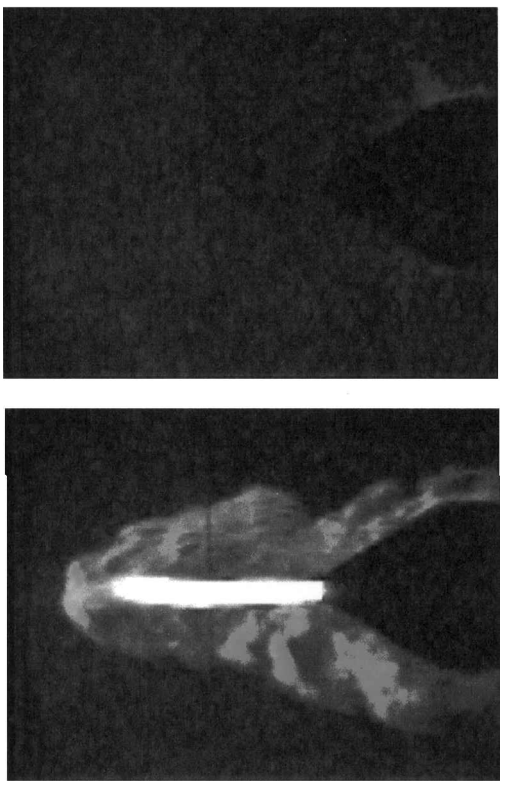

Fig. 6 Shadowgraphs at $M_\infty = 0.59$ prior to (top) and at the instant of plasma discharge.

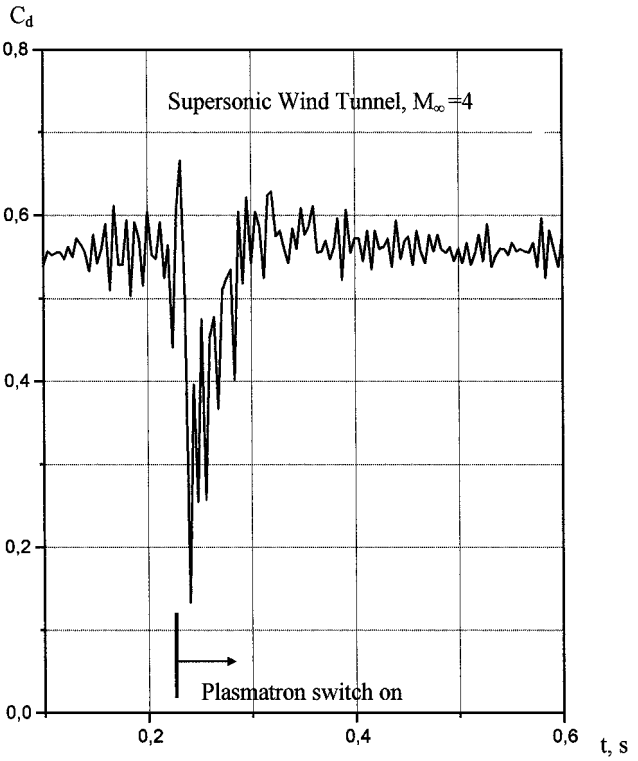

Fig. 7 Time dependence of C_d for plasma flowing at $M_\infty = 4$.

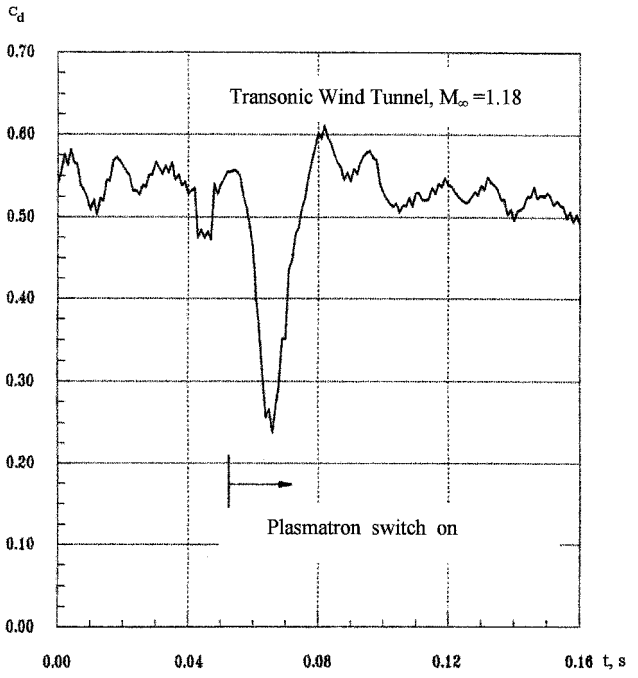

Fig. 8 Time dependence of C_d for plasma flowing at $M_\infty = 1.18$.

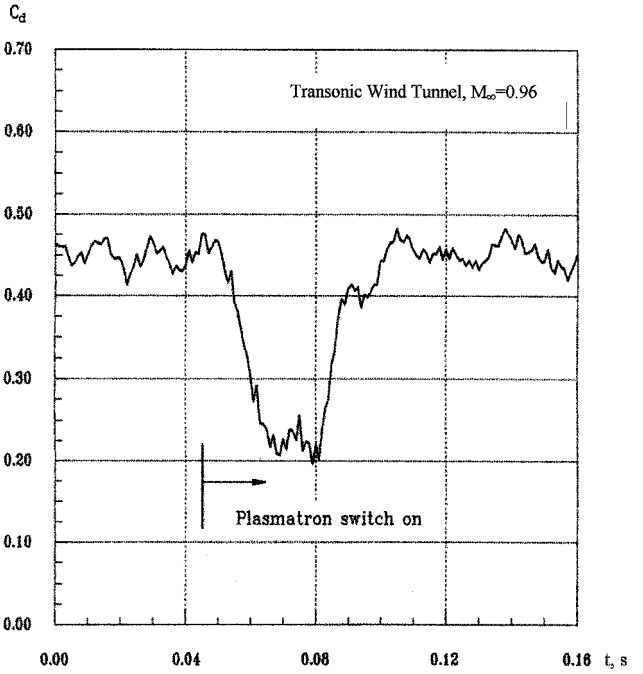

Fig. 9 Time dependence of C_d for plasma flowing at $M_\infty = 0.96$.

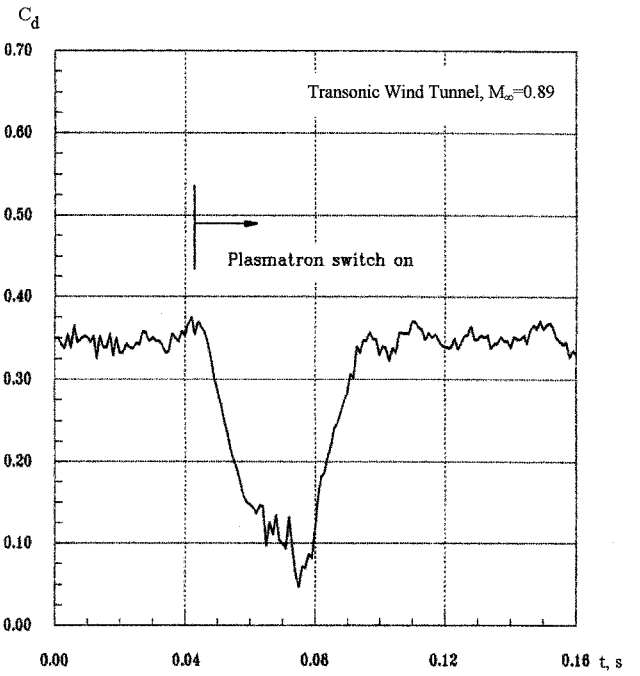

Fig. 10 Time dependence of C_d for plasma flowing at $M_\infty = 0.89$.

to and after plasma discharge. The model-sting system oscillations lead to the relative high-frequency curve oscillations.

The plasma jet thrust, evaluated using the measured pressure in the plasma generator chamber, the geometric parameters of the nozzle, and a rough value of plasma stagnation temperature of 6000 K, amounted to from 5 to 10% of the total aerodynamic force.

By studying Figs. 7–11, one can see that the plasma generator working time changed from 3 to approximately 10 ms in the different tests. Maximum working time ~10 ms corresponds with Mach 4. In this case the nozzle throat diameter was minimum ($d = 2$ mm).

The largest drag reduction (about four times) is observed at Mach 0.89 (Fig. 11).

By using the experimental results of Figs. 7–11, the Mach number dependence of C_d was plotted (Fig. 12). The dotted lines are an approximation of the experimental data there.

After a careful analysis of Fig. 12, we can conclude that plasma injection technology can be developed to reduce aerodynamic drag at subsonic, transonic, and supersonic Mach numbers. Thus, the presented technology can be used to destroy or to reduce greatly the effects of the sonic barrier. However, to achieve this purpose the investigation of optimum results must be carried out.

Model with Built-In Solid Fuel Gas Generator

To study the possibility of reducing aerodynamic drag by use of a different method, we designed and manufactured a cone–cylinder

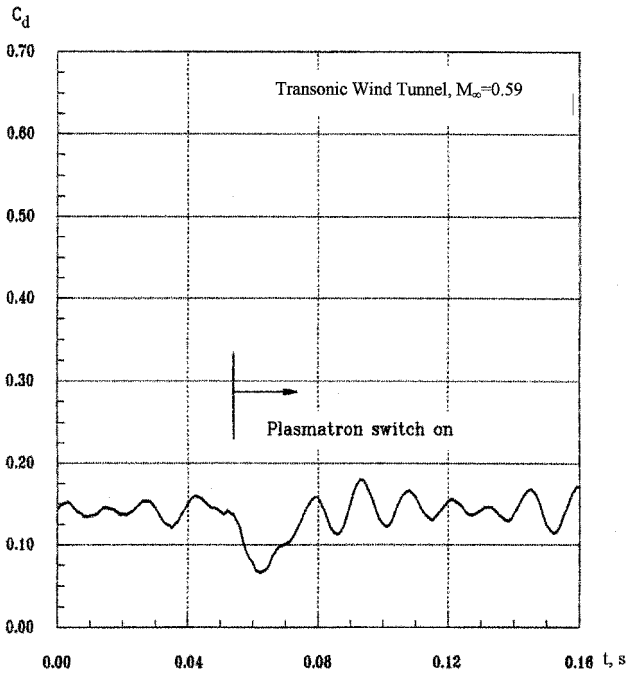

Fig. 11 Time dependence of C_d for plasma flowing at $M_\infty = 0.59$.

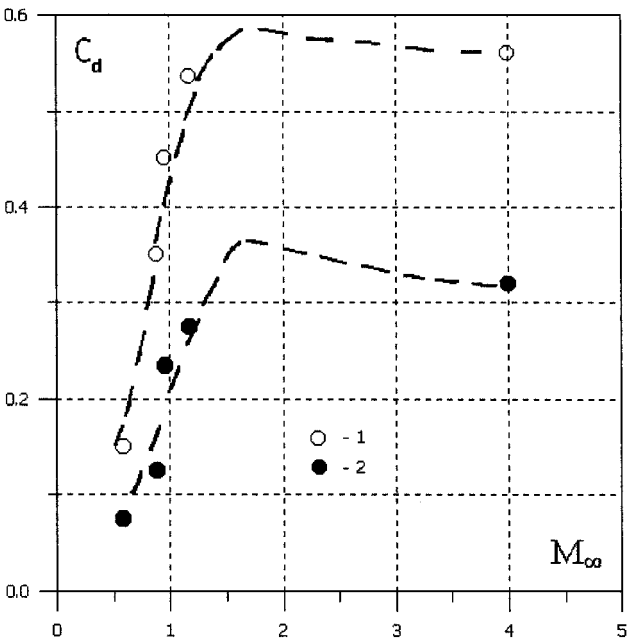

Fig. 12 Mach number dependence of C_d: 1, without plasma flowing; 2, with plasma flowing; and – – –, approximation.

model with a built-in solid fuel gas generator and strain gauges. The model and strain gauges were the same as before (Fig. 1), but the solid fuel gas generator replaced the plasma generator.

The solid fuel gas generator was mounted on a sting installed in the wind tunnel working section, and the model-tubular strain gauge assembly was fitted on it. The general parameters of the solid fuel gas generator are as follows: The working section is up to 120 mm, the inner diameter of the gas generator chamber is 30 mm, the cylinder wall thickness is 4 mm, the nozzle throat diameters are 4 and 5 mm, the exit diameters are 7.61 and 8.6 mm, and the length and the diameter of the solid fuel cartridge are 48 and 25 mm, respectively.

The gas generator uncooled nozzles were made of tungsten. The temperature of solid fuel burning was about 3000 K, and the time of burning was from 4 to 8 s. At such conditions copper begins to melt. The pressure in the hot gas generator chamber also was measured using a DMI inductive transducer. To ignite the solid fuel, 27 V dc are fed to the initial charge in front of the solid fuel cartridge.

Experimental Results for Model with Built-In Solid Fuel Gas Generator

The tests were carried out in the supersonic wind tunnel at Mach 3 and stagnation pressure of 3.5 atm. Figure 13 shows as an example of the flow patterns prior to and at the instant of hot gas flowing after the solid fuel burning. The experiments were carried out with a nozzle throat diameter of 4 mm. The photographs were taken using an IAB-451 shadowgraph and a movie digital color camera shooting 100 frames per second with an exposure at about 167 μs. In this case, one can see the significant flow picture reconstructing at the instant of hot gas flow, with decomposition of the original bow shock wave and formation of a new shock wave configuration. The working time of the hot-gas injection was about 8 s.

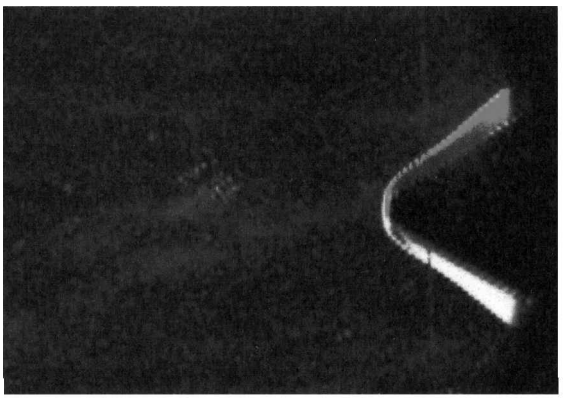

Without hot gas flowing, $t = 0$

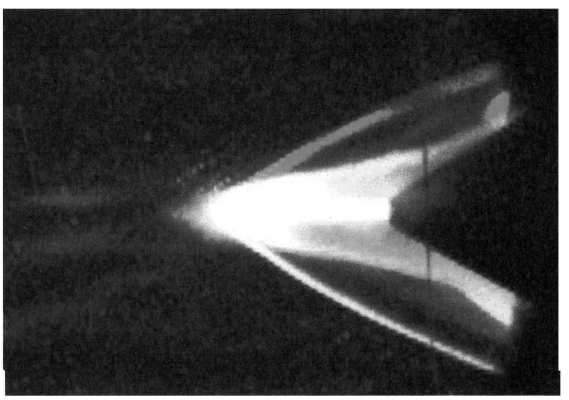

With hot gas flowing, $t = 0.64$ s

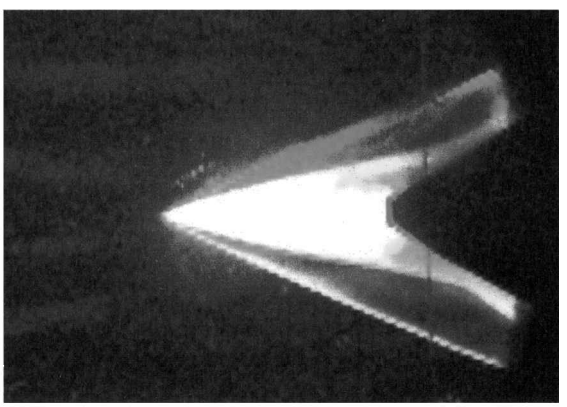

With hot gas flowing, $t = 7.07$ s

Fig. 13 Shadowgraphs of the flow at $M_\infty = 3$.

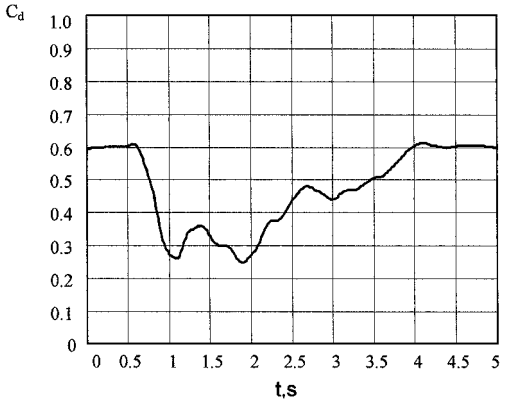

Fig. 14 Time dependence of C_d for hot gas flowing at $M_\infty = 3$.

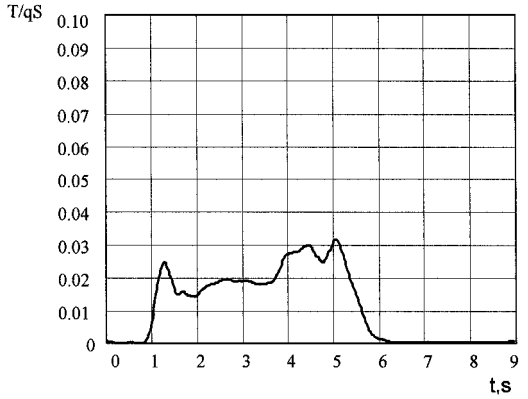

Fig. 15 Time dependence of dimensionless thrust T/qS without external flow for hot gas flowing.

By comparison of Figs. 2 and 13 at the moment of plasma and hot-gas injection, one can note that the formation of the shock wave configurations is different. The hot-gas injection forms a sharper shock wave configuration than plasma injection.

Figure 14 shows the time dependence of C_d during the experiment, when the nozzle throat diameter was 5 mm. Maximum drag reduction is about two times greater in this case, and the working time of the hot-gas injection is about 3.5 s. Figure 15 demonstrates the time dependence of the dimensionless thrust T/qS for the hot gas flowing through a nozzle throat diameter of 5 mm. In this case the model was fastened and the gas generator was unfastened from supporting device. The test was carried out in the wind tunnel without external flow. By comparison of Figs. 14 and 15, one can conclude that maximum thrust is about 10% of the value of the drag reduction. Thus, in this case the positive effect of the drag reduction is rather significant.

Computational Simulations

To understand the physics of the drag reduction in the wind-tunnel experiments, numerical experiments were conducted. A computer program was written, and preliminary calculations of the symmetrical flow near the body cone–cylinder at $M_\infty = 4$ were conducted for the injection of very hot and medium hot gas into the oncoming supersonic flow. The hot-gas Mach number was $M_j = 3.65$, and the stagnation pressure was $p_{0j} = 15.4$ atm in all cases.

The following dimensional (dimensionless) parameters of the oncoming flow at a stagnation pressure of $p_0 = 12$ atm and a stagnation temperature of $T_0 = 290$ K were used: $\rho_\infty = 0.4$ kg/m^3 (1), $V_\infty = 666$ m/s (1), and $p_\infty = 0.079$ atm (0.0446). The specific heat ratio $\gamma = 1.4$ was constant, and the characteristic values for the dimensionless flow parameters were density ρ_∞, velocity V_∞, and length $L = 1$ mm. Three cases with the same jet impulse but different jet stagnation temperatures, $T_{0j} = 6000$, 2000, and 600 K, were calculated. The dimensionless parameters of the jet at the nozzle exit are given in Table 2.

Table 2 Dimensionless parameters of jet at the nozzle exit

	T_{0j}, K		
Parameter	6000	2000	600
ρ_j	0.0865	0.2602	0.8675
V_j	4.4	2.565	1.4
p_j	0.0918	0.0918	0.0918

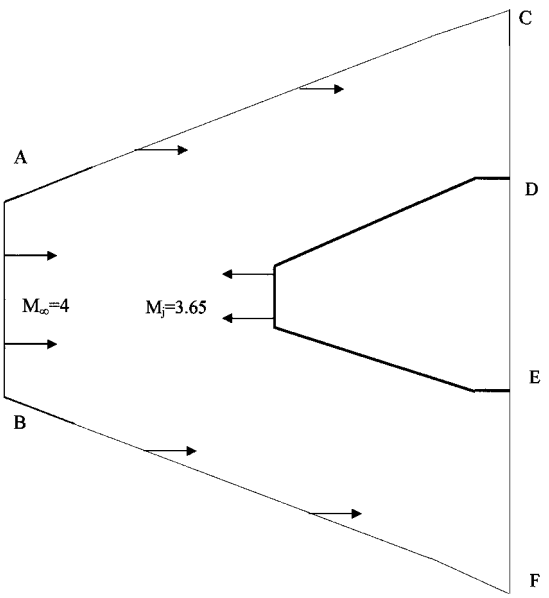

Fig. 16 Flow scheme.

Figure 16 presents the flow scheme. The boundary conditions were as follows: on lines AB, AC, and BF, uniform freestream flow; on the symmetry axis, symmetrical conditions of flow; on the outside of boundaries CD and EF, free out; on the cone–cylinder surface, $U_n = 0$, where U_n is the normal component gas velocity to the body surface; on the cone nose, parameters of injecting gas at the nozzle exit.

The unsteady Euler equations of the ideal perfect gas in integral conservative form were considered for the mathematical model, and the well-known McCormac difference scheme was used. In the places where flow instability appeared, the solution was smoothed.[14] During the calculation process, the shock waves were not especially noted.

The dimensionless time step Δt was determined from Courant stability conditions. The meshes used included 100×100 points. The calculations were finished when the differences of relative flow parameters at the neighboring time steps were less than 0.01.

Figures 17 and 18, as examples, show the computed pressure, density, temperature, and Mach number distributions at stagnation temperatures $T_{0j} = 6000$ and 600 K, respectively. The results are presented as color fields of small regions p, ρ, T, and $M = \text{const}$. The values of the parameters are an average for those small regions. Let us consider the computed results for hot-gas injection at $T_{0j} = 6000$ K. Figure 17 shows that the pressure and the density near the critical point are small in comparison with the values without hot-gas injection. Those, as well known, are approximately equal to 0.92 and 3.7, respectively. The jet temperature is about 1100 K at the initial and middle parts, and at the end the temperature increases to ~2900 K. Here the jet is separated by the contact surface. Near the stagnation point, one can see the hot region with temperature ~6000 K and pressure ~0.9. The high-pressure region is localized, and the flow with temperatures ~4500–5000 K cover a rather long region.

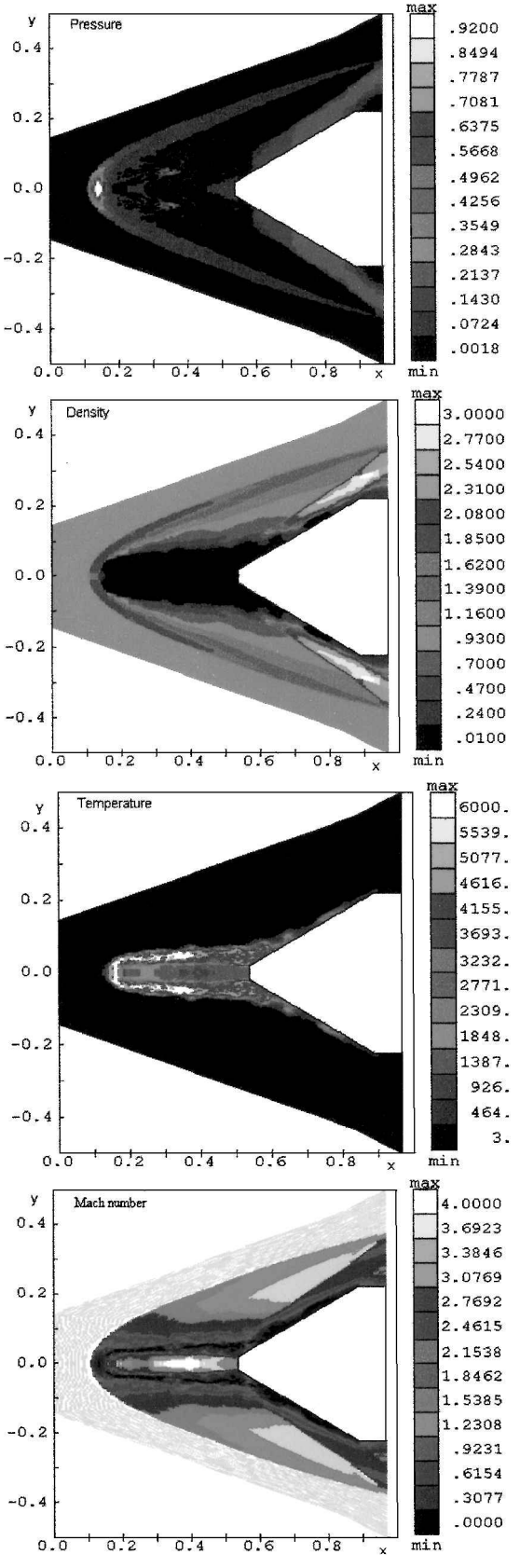

Fig. 17 Pressure, density, temperature, and Mach number distributions at stagnation temperature $T_{0j} = 6000$ K.

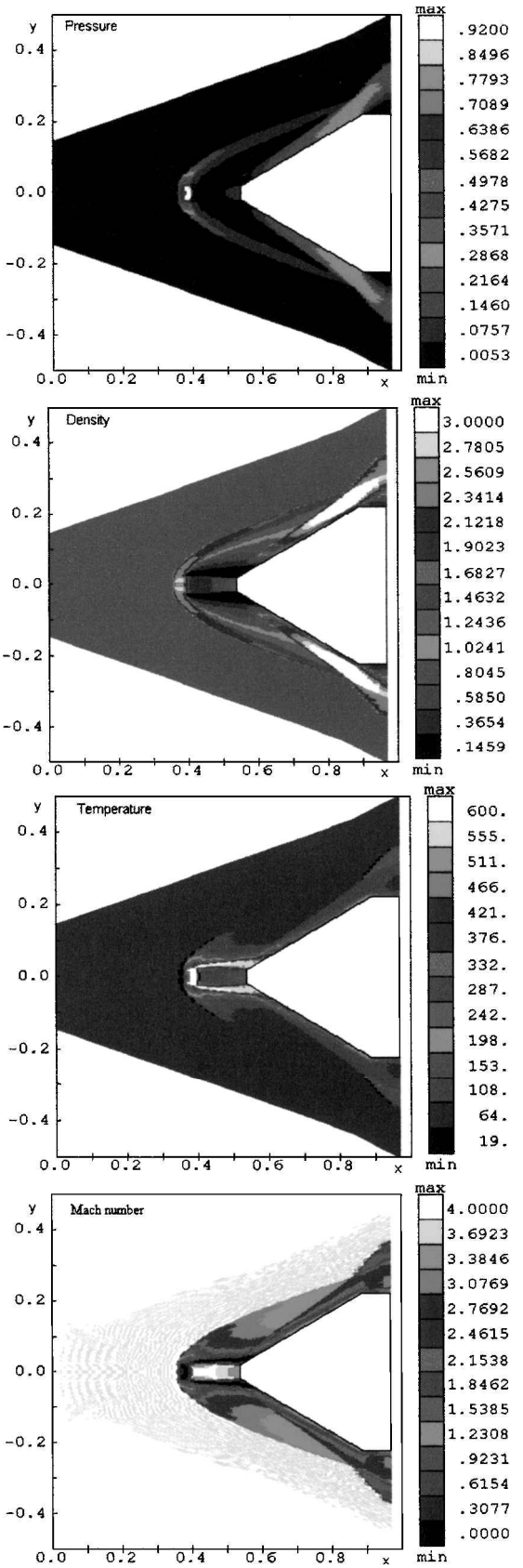

Fig. 18 Pressure, density, temperature, and Mach number distributions at stagnation temperature $T_{0j} = 600$ K.

Table 3 Stagnation hot-gas temperature dependence of C_d

T_{0j}, K	C_d
Without gas injecting	0.56
600	0.52
2000	0.45
6000	0.32

Near the stagnation point, the hot jet turns around, separated from the involved gas by a second contact surface, which is separated by the next contact surface from external flow. Between the first and second contact surfaces, the gas initially moves with supersonic velocity and subsonic velocity near the external contact surface. The flow between second and third contact surfaces is subsonic. Near the jet stagnation point, the bow shock wave forms. The flow following it is subsonic and then supersonic. In fact, the oncoming flow moves almost as if it is a liquid body. This flow is supersonic except in the stagnation point region.

The gas flow from the jet has a small density of ~ 0.1. This gas flow consists of two parts near the meeting of the second contact surface with the cone. The first part of the flow returns and forms a closed-flow region. The second part of the flow is near the cone surface and forms a fictitious liquid body with smaller angle, respectively, to the oncoming supersonic flow. Here the pressure value is ~ 0.2–0.3 and the density is small, but the temperature is high. The pressure increases as a result of the external supersonic flow slowing. Its slowing causes a shock to form near the cone surface.

By analyzing and comparing Figs. 17 and 18, one can conclude that all higher pointed structure flow elements for $T_{0j} = 6000$ K take place for $T_{0j} = 600$ K. However, for $T_{0j} = 600$ K the sizes of interaction regions are smaller because in that case the kinetic energy stream, determined as $\rho_j V_j^3/2$, is smaller because $V_j \sim T_{0j}^{1/2}$. Having smaller kinetic energy, the jet also has a smaller penetration range. The pressure value at the cone surface is significantly greater in that case. As a result, drag reduction is less.

In Table 3 the computed results for the hot-gas stagnation temperature dependence of C_d are presented. In Table 3 one can see that the value of drag reduction depends on jet stagnation temperature. Also note that the value of drag reduction for $T_{0j} = 6000$ K is quite near the experimental results at $M_\infty = 4$ with plasma injection (Fig. 7).

Conclusions

The influence of plasma and hot-gas injection from a cone–cylinder model surface toward the external flow on the aerodynamic drag of the model has been studied. The experimental and theoretical investigations showed that the plasma and hot-gas injection can be used to reduce drag at subsonic, transonic, and supersonic Mach numbers. Therefore, technology can be developed to destroy or at least to reduce the effects of the sonic barrier and, possibly, to help overcome the hypersonic barrier (the design and realization of high-speed civil transport).

The value of the drag reduction depends on the jet stagnation temperature. The experimental and theoretical results are in agreement.

The drag reduction at supersonic velocities can be explained as a result of the formation, near the model, of an effective liquid body with the low pressure and density values.

The flow pictures with plasma and hot-gas injection are different.

Further investigations are required to explain the effect of the drag reduction at subsonic and transonic Mach numbers. In addition, it is necessary to understand the influence that plasma and hot-gas physics properties have on the drag reduction.

References

[1]Krasnov, N. F., Koshevoi, V. N., and Kalugin, V. T., "Separated Flow Aerodynamics," Vysshaya Skola, Moscow, 1988 (in Russian).

[2]Artem'ev, V. I., Bergelson, V. I., Nemchinov, I. V., Orlova, T. I., Smirnov, V. I., and Khazins, V. M., "Variation in the Mode of Supersonic Flow Past an Obstacle due to the Formation of a Narrow Rarefied Channel Ahead of It," *Izvestia, Academy of Sciences USSR, Mekh. Zhidk. Gasa*, No. 5, 1989, pp. 146–151.

[3]Georgievskii, P. Y., and Levin, V. A., "Supersonic Flow Past Bodies in the Presence of External Heat Release Sources," *Pis'ma Zhurnal Teknicheskoi, Fiziki*, Vol. 14, No. 8, 1988, p. 684.

[4]Candler, G. V., Kelley, J. D., "Effect of Internal Energy Excitation on Supersonic Blunt-Body Drag," AIAA Paper 99-0418, Jan. 1999.

[5]Pankova, M. B., Leonov, S. B., and Shipilin, A. V., "Simulation of the Specific Feature of the Interaction of Ball Lighting with the Physical Phenomena Accompanying the Flight of Bodies Through the Atmosphere," *Ball Lighting in the Laboratory*, Khimiya, Moscow, 1994, p. 95 (in Russian).

[6]Gridin, A.Y., Efimov, B. G., Zabrodin, A. V., Klimov, A. I., and Kuzin, K. A., "Calculation-Experimental Study of Supersonic Flow Past a Blunt Body with a Needle in the Presence of an Electrical Discharge near the Nose," Preprint No. 19, M. V. Keldysh Inst. of Applied Mathematics, Russian Academy of Sciences, 1995 (in Russian).

[7]*Proceedings of the 1st Workshop of Weakly Ionized Gases*, U.S. Air Force Academy, Colorado Springs, CO, June 1997.

[8]*Proceedings of the 2nd Workshop of Weakly Ionized Gases*, AIAA, Reston, VA, 1998.

[9]Finley, P. J., "The Flow of a Jet from a Body Opposing a Supersonic Free Stream," *Journal of Fluid Mechanics*, Vol. 26, Pt. 2, pp. 337–368.

[10]Ganiev, Y. G., Gordeev, V. P., Krasilnikov, A. V., Lagutin, V. I., and Otmennikov, V. N., "Experimental Study of the Possibility of Reducing Supersonic Drag by Employing Plasma Technology," *Fluid Dynamics*, Vol. 31, No. 2, Consultants Bureau, New York, 1996; translated from *Izvestia Rossiiskoi Akademii Nauk, Mekhanika Zhidkosti i Gasa*, No. 2, 1996, pp. 177–182.

[11]Ganiev, Y., Gordeev, V., Krasilnikov, A., Lagutin, V., and Otmennikov, V., "Experimental Study of the Possibility of Reducing Aerodynamic Drag by Employing Plasma Injection," *Proceedings of the Third International Conference on Experimental Fluid Mechanics*, Korolev, Moscow Region, Russia, June 1997.

[12]Ganiev, Y. G., Gordeev, V. P., Krasilnikov, A. V., Lagutin, V. I., Otmennikov, V. N., and Panasenko, A. V., "Experimental and Theoretical Study of the Possibility of Reducing Aerodynamic Drag by Employing Plasma Injection," *Proceedings of the 2nd Workshop of Weakly Ionized Gases*, Norfolk, VA, 1998.

[13]Ganiev, Y. G., Gordeev, V. P., Krasilnikov, A. V., Lagutin, V. I., Otmennikov, V. N., and Panasenko, A. V., "Theoretical and Experimental Study of the Possibility of Reducing Aerodynamic Drag by Employing Plasma Injection," AIAA Paper 99-0603, Jan. 1999.

[14]Rizzi, A. W., and Inouye, M., "Timesplit Finite Volume Method for Three-Dimensional Blunt Body Flow," *AIAA Journal*, Vol. 11, 1973, pp. 1478–1485.